

## Synthesis of functional TiO<sub>2</sub>-based nanoparticles in radio frequency induction thermal plasma\*

Takamasa Ishigaki<sup>‡</sup> and Ji-Guang Li

*Nano Ceramics Center, National Institute for Materials Science, Namiki, Tsukuba, Ibaraki 305-0044, Japan*

*Abstract:* A method of synthesizing functional nanostructured powders by using reactive thermal plasma processing has been developed. Nanosized TiO<sub>2</sub> powders have been synthesized by the plasma oxidation of solid and liquid precursors. Quench gases, either injected from the shoulder of the reactor or injected counter to the plasma plume from the bottom of the reactor, are used to affect the quench rate and hence the particle size of the resultant powders. The experimental results are well supported by numerical analysis of the effects of the quench gas on flow pattern and temperature field of the thermal plasma as well as trajectory and temperature histories of the particles. The plasma-synthesized TiO<sub>2</sub> nanoparticles showed phase preferences different from those synthesized by conventional wet processes. Nanosized particles of high crystallinity and nonequilibrium chemical composition were formed in one step by reactive thermal plasma processing. The plasma-synthesized nanoparticles were spherical and hardly agglomerated. Applications of highly functional nanoparticles are thought to require nanoparticles structured in the forms of (1) dispersoids, (2) fillers, and (3) patterns. For these purposes, plasma-synthesized nanocrystallites seem to be suitable.

*Keywords:* nanosized particles; thermal plasma processing; particle size control; phase formation; reactor design.

### NANOPARTICLE SYNTHESIS

Nanoparticles offer one possibility for the breakthrough needed to advance the conversion of substances into materials. When looking forward to the development of nanoparticles, we can describe the advantages of nanoparticles from two viewpoints. One is the so-called “nanosize effect” expected in physical properties such as luminescence or chemical properties such as catalytic activity. The other is the effect on precious materials conservation, which reduces the volume of materials required for functionalization. In both cases, the fundamental idea is to homogeneously produce highly functional substances in large quantities. If this is achieved, the development of nanoparticles will be possible.

The present situation, however, is that the nanoparticles synthesis field is still under development. To utilize these properties effectively, it will be important to control the crystallinity and surface properties as well as the homogeneity of crystallite size and chemical composition in association with the development of high-throughput processes.

---

\*Paper based on a presentation at the 18<sup>th</sup> International Symposium on Plasma Chemistry (ISPC-18), 26–31 August 2007, Kyoto, Japan. Other presentations are published in this issue, pp. 1883–2023.

<sup>‡</sup>Corresponding author

Nanosized powder synthesis should be oriented to achieve precise control of the particle size, morphology, and chemical composition, and crystal structure. A monodispersed powder is defined to have a standard deviation of below 10 %. Up to now, only a few kinds of wet chemically synthesized nanopowders have satisfied this requirement. The morphology and chemical composition of particles are closely related to the assembly of particles and their functionalization. Control of surface properties is essential to the application of nanoparticles in functional ordered-arrays. Dispersed structures also need controlled surface properties.

Nanoparticle synthesis of ceramic materials has conventionally been achieved using solution processes. Taking the example of luminescence properties, major factors that have hindered the functionalization of solution-synthesized oxide nanoparticles include low crystallinity, quenching by surface hydroxyl groups, and incomplete composition control (doping concentration, surface segregation). Moreover, the existence of surface hydroxyls is known to have a big impact on the dispersion of nanoparticles in a solvent.

In this review of our recent and current investigations, we first describe thermal plasma materials processing methods and their characteristics and then describe their advantages in nanoparticle synthesis. Next, we present our research achievements with the aim of showing how to utilize highly functional nanoparticles synthesized with plasma. Finally, we discuss the outlook for nanoparticle applications.

## SYNTHESIS OF NANOPARTICLES IN REACTIVE THERMAL PLASMAS

Thermal plasmas possess many advantages and provide unique reaction fields for materials processing. The improved controllability of the reaction fields, in which chemical reactions proceed to yield materials, should lead to the synthesis of unique materials with respect to morphology, crystal structure, and chemical composition. Arc discharge, which is the so-called thermal plasma, has proved to be a useful tool in the synthesis and surface modification of a wide range of metals and inorganic materials. The advantages of thermal plasmas as reaction fields are as follows: (1) Thermal plasmas have extremely high temperatures (up to 15 000 K). As the plasmas are generated at relatively high pressures (close to atmospheric pressure), they have high densities and are considered to be at equilibrium (local thermal equilibrium). That is, the temperatures of heavy particles (such as atoms, molecules, and ions) are almost equal to those of the light species (that is, electrons). (2) High concentrations of chemically reactive radicals enhance the reactivity of the thermal plasmas. (3) Superfast quenching ( $<10^5$  to  $<10^6$  K/s) takes place in the plasma tail flame region.

A representative use of thermal plasma processing is the spheroidization of materials with high melting temperatures and large particle sizes (such as 50–100  $\mu\text{m}$ ) [1]. For example, titanium carbide has an extremely high melting point, ca. 3350 K, so the TiC powder can be in-flight spheroidized in a short time [2]. Industrially, 30 kg of refractory tungsten metal particles can be treated per hour, which corresponds to 1 ton per week [3]. As thermal plasma processing has these inherent characteristics, that is, processing at an industrially acceptable production rate, the ongoing work on nanostructure control of materials using thermal plasma technology should lead to practical use in a short time.

The route of nanoparticle formation in radio frequency (RF) induction thermal plasma is shown in Fig. 1. Nanosized particles are formed by a process of rapid quenching and condensation after precursors are supplied into the thermal plasma and are instantaneously evaporated. The rapid temperature decrease in the tail flame gives rise to supersaturation in the vapor phase, and then the nucleation process takes place. In the same way, the rapid cooling suppresses grain growth, so nanoparticles smaller than 100 nm in size are produced without difficulty. Advanced technologies should be pursued to control the plasma reaction fields to yield (a) high production rates, (b) smaller particle sizes and narrower size distributions, and (c) high crystallinity and phase control. Practical applications of nanosized particles will be possible once such technologies have been developed.

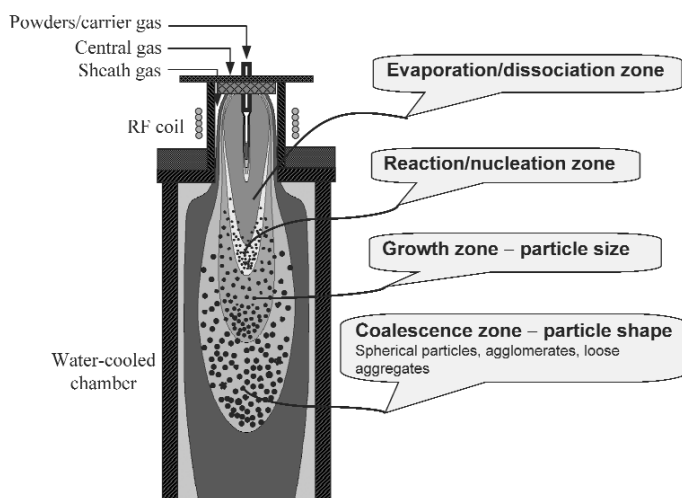


**Fig. 1** Formation of nanoparticles in RF induction thermal plasma.

Nanoparticle production by utilizing the advantages of thermal plasmas, i.e., high-temperature heat source with tremendously high enthalpy, was started with the use of solid-state precursors. Relatively coarse particles were introduced into thermal plasmas to synthesize nanosized particles through evaporation and the subsequent coagulation processes. In this production method, problems come from the residual coarse particles. When precursor powders are injected into a thermal plasma, in which the temperature and flow distributions exist both radially and axially, some of the precursor particles are not completely evaporated. The non-evaporated part, though small, necessitates an additional post-separation process [4–6].

To solve the problem of solid precursor processing and to produce uniform nanosized particles, liquid precursors have been used [7,8]. When a mist with a droplet size on the order of 10  $\mu\text{m}$  is fed into a plasma having a temperature above 10 000  $^{\circ}\text{C}$ , the mist vaporizes instantaneously, enabling mass production of nanoparticles. Oxides with the prescribed cation ratio of the liquid precursor itself can be synthesized by this technique. It is also possible to control the chemical composition, which is linked to the appearance of functions. Nonequilibrium compositions and structures have been observed in nanoparticles as a result of rapid cooling at the plasma tail flame. These are extremely interesting phenomena from the scientific viewpoint.

## SIZE CONTROL OF NANOPARTICLES IN RF INDUCTION THERMAL PLASMAS

The effects of processing parameters have been investigated in the synthesis of TiO<sub>2</sub> nanoparticles by Ar/O<sub>2</sub> RF thermal plasma oxidation of liquid precursor mists.

Nanoscale size control of particles is crucial to the functions, in view of the quantum size effects in catalytic, electrical, magnetic, and optical properties. Also, a narrower size distribution should extend the application area. The easiest and most effective way to produce uniform nanosized particles is to allow chemical reactions to proceed under dilute conditions. On the other hand, practical process-control should be performed under high precursor loading conditions.

Nucleation from a gas phase and subsequent grain growth take place in the plasma tail. Therefore, size control should be performed by modifying the temperature and flow distribution downstream of the plasma. We have demonstrated the particle-size-controlled synthesis of well-dispersed TiO<sub>2</sub> nanopowders by Ar/O<sub>2</sub> thermal plasma oxidation of liquid precursor mists, by manipulating the cooling rates by injecting quench gases (Ar, He) [9]. In that case, the TiO<sub>2</sub> nanoparticles were synthesized by Ar/O<sub>2</sub>

thermal plasma oxidation of atomized liquid precursors containing titanium tetrabutoxide (TTBO, the titanium source) and diethanolamine (a chelate preventing the hydrolysis of TTBO). RF power at a frequency of 2 MHz and a power level of 25 kW was used to generate plasma at a pressure of 53.3 kPa. The precursor was atomized into mist at the tip of the atomization probe by Ar carrier gas flowing through the probe. The feed rate of the liquid precursor was controlled at  $4.5 \text{ g}\cdot\text{min}^{-1}$ , which corresponds to  $4.5 \times 10^{-3} \text{ mol}\cdot\text{min}^{-1}$ .

Quench gas was injected in two different ways: transverse injection (Fig. 2a) and counter injection (Fig. 2b). The morphologies of  $\text{TiO}_2$  powders synthesized with and without Ar quench gas injections are compared in Fig. 3. X-ray diffraction showed that the synthesized powders consisted of the rutile and anatase phases of  $\text{TiO}_2$ . The majority of the particles assumed rounded shapes, with sizes ranging from a few nanometers to about 200 nm. The plasma-generated particles showed weak agglomerations, which is in sharp contrast to those synthesized by most wet-chemical techniques.

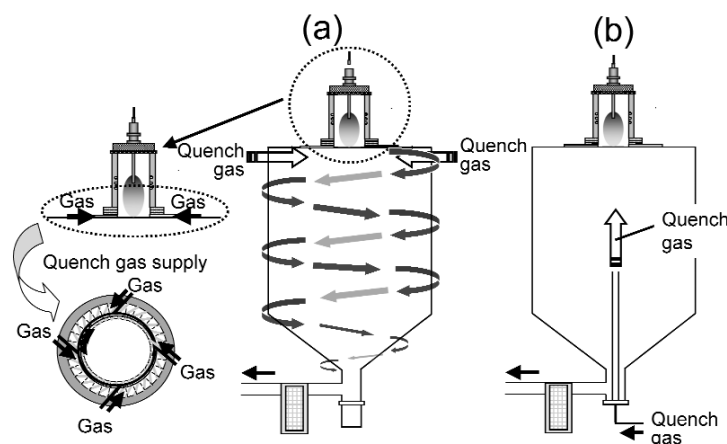


Fig. 2 Experimental set-ups for transverse swirl-flow injection (a) and counter-flow injection (b) of quench gases.

The overall morphology of the powder was not significantly altered by injecting 100 l/min of Ar in the transverse mode (Fig. 3b), but the powder became appreciably finer when the same amount of Ar was injected in the counter-flow mode (Fig. 3c), revealing the significance of the quenching method on powder properties. Size distributions of the powders were evaluated by image analysis of SEM (scanning electron microscope) photos. Powders synthesized without quench gas and with Ar transverse flow were found to have similar  $d_{50}$  values of about 55 and 53 nm, respectively. Powder made with the Ar counter flow had a considerably smaller distribution of about 35 nm.

Modeling has been performed to better understand the effects of quench gases and to optimize the process parameters and reactor design [9]. Since the particles are synthesized from the vapor phase of the precursors, their trajectories should follow the streamlines of the fluid due to the small masses of the particles. As a simplified approach, we trace the motion of a test particle with negligible mass and infinite melting point in the plasma flow, indicating that the nanosize particle moves with the plasma at the same velocity and temperature. The calculated particle trajectory and temperature history are expected to qualitatively describe the effect of the quench gas.

The calculated streamlines and temperature fields in the reactor are shown in Fig. 4. The dots in Fig. 4 indicate the predicted trajectory of a test particle released at the tip of the central probe. Comparing Figs. 4a and b, we can see that transversely injecting Ar did not significantly alter the temperature fields of the plasma or the trajectory of the test particle. When Ar was injected counter to the plasma plume, on the other hand, it profoundly affected the temperature field and also the particle trajectory (Fig. 4c). The greatly decreased size of the plasma plume allowed the particle to have a shorter

duration in the high-temperature zone, which favored finer particle formation. The above numerical analysis results support the experimental data given in Fig. 3 well.

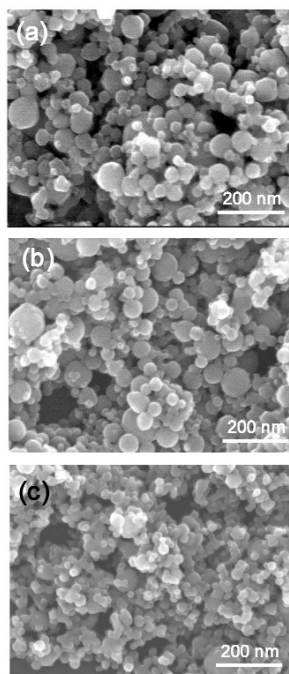


**Fig. 3** SEM micrographs showing morphologies of the TiO<sub>2</sub> powders synthesized (a) without the use of quench gas, (b) with transverse swirl-flow injection of 100 l/min of Ar, and (c) with counter-flow injection of 100 l/min of Ar.

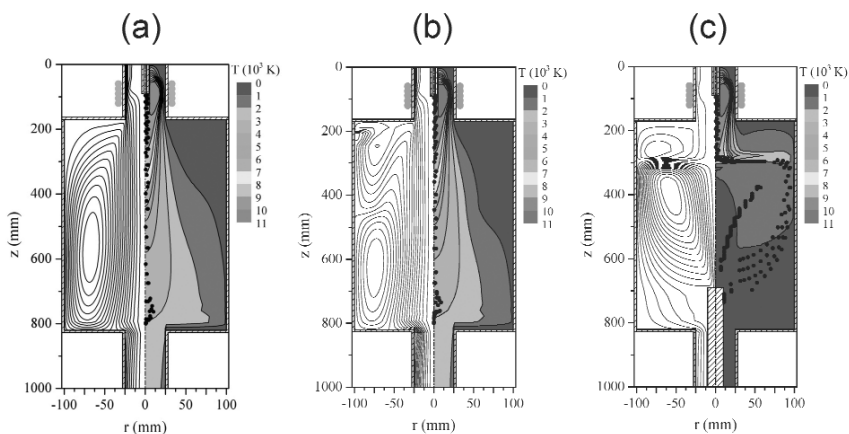


**Fig. 4** Streamlines and temperature distribution for (a) no quench gas, (b) transverse swirl-flow injection of Ar at 100 slpm, and (c) counter-flow injection of Ar at 100 slpm.

## PHASE SELECTION AND FORMATION OF NONEQUILIBRIUM CHEMICAL COMPOSITION IN TITANIUM OXIDE NANOPARTICLES

TiO<sub>2</sub>, which has classically been used as a white pigment, exhibits interesting properties, such as high transparency in the visible wavelength region, high refractive index, and remarkable chemical and thermal stabilities. These have led to new applications for it in photocatalysis, solar cells, semiconducting gas sensors, biosensors, and as a building block for photonic crystals. For its use as a photocatalyst, the doping of TiO<sub>2</sub> with nitrogen and transition-metal ions has been shown to be an effective method of enhancing the photocatalytic activity under visible light irradiation, which extends the applications to indoor uses. Recently, transition-metal-doped TiO<sub>2</sub> has been extensively studied for its potential application as a ferromagnetic semiconductor because room-temperature ferromagnetic properties have been reported in Co-doped TiO<sub>2</sub> thin films.

In a high-temperature thermal plasma, highly crystalline nanosized particles with doping modifications are formed by one-step processing, without post-heat treatment. We have reported the synthesis of TiO<sub>2</sub> particles by the plasma oxidation of TiC [4,10] and TiN [11] powder precursors. In the powder oxidation method, a very high degree of supersaturation is attained in the vapor phase compared with vapor-phase precursor processing. Thus, TiO<sub>2</sub> particles of micrometer/submicrometer/nanometer size were formed depending on the degree of supersaturation in the vapor phase [4,10]. TiO<sub>2</sub> is known to have two common polymorphs: anatase and rutile.

Interestingly, the thermodynamically metastable anatase predominated the undoped TiO<sub>2</sub> nanopowders, which can be explained from the viewpoint of kinetics based on classical homogeneous nucleation theory, in which the critical nucleation energy,  $\Delta G^*$ , was evaluated for the rutile and anatase phases [12,13]. The estimation of  $\Delta G^*$  was performed using the Gibbs free energy data and the estimated interfacial energies between the liquid and solid phases of TiO<sub>2</sub> based on the theory using an elementary nearest-neighbor-atoms approach.

On the other hand, decreasing the oxygen partial pressure in the vapor phase gave pure rutile nanoparticles [10]. Decreasing the oxygen partial pressure promoted the formation of oxygen-deficient rutile nanopowder. Because oxygen vacancies carry a positive charge, rutile has greater tolerance than anatase toward oxygen vacancies due to fewer shared edges in the crystal structure of rutile. Crystal chemical theory suggests that shared edges should lead to cation–cation repulsion and structural destabilization, in accordance with the relative stability of both phases.

Next, liquid mixtures, in which some metal elements exist as ions in aqueous solutions or as constituent atoms of metallorganic compounds, were used as the precursors. The use of liquid precursors enables uniform nanoparticles to be formed and has the advantages of a high production rate. Precise control of chemical composition also provides the opportunity to get particles with nonequilibrium doping, in which the doping quantity is higher than the solubility limit under equilibrium conditions.

TiO<sub>2</sub> nanoparticles have been synthesized by Ar/O<sub>2</sub> thermal plasma oxidation of atomized liquid precursors. In the case of iron doping, mixtures of TTBO and ferrocene dissolved in ethanol were used as precursors. The liquid precursor for europium doping was made by the following procedure: TTBO was added to diethanolamine to stabilize the TTBO against hydrolysis. Separately, europium nitrate and citric acid were dissolved in water, and the pH of the solution was adjusted to 9.0 by using ammonia solution. Mixing these two solutions yielded a stable clear solution to be used as the liquid precursor. The feed rate of the liquid precursor was controlled at 5.4 and  $4.5 \times 10^{-3}$  mol·min<sup>-1</sup> for iron and europium-doped TiO<sub>2</sub>, respectively.

In iron-doped TiO<sub>2</sub> nanoparticles, no other phases except anatase and rutile TiO<sub>2</sub> were identified for a wide range of iron-to-titanium atomic ratios ( $R_{\text{Fe/Ti}}$ ) ranging from 0 to 0.2, though the solubility of iron in TiO<sub>2</sub> was reported to be around 5 at % for conventional wet processes. With iron doping, the formation of rutile was strongly promoted because rutile is more tolerant than anatase of defects such as oxygen vacancies that result from the substitution of Fe<sup>3+</sup> for Ti<sup>4+</sup> in TiO<sub>2</sub>. The concentration of oxygen vacancies reached its maximum at  $R_{\text{Fe/Ti}} = 2$  %. Above that, the excess oxygen vacancies

tended to concentrate. As a result of this clustering, an extended defect like a crystallographic shear structure was established, as shown by the high-resolution transmission electron microscope (HRTEM) image in Fig. 5 [13]. The highly iron-doped TiO<sub>2</sub> nanocrystals showed paramagnetic properties. Fe<sup>3+</sup> substituted for Ti<sup>4+</sup> and was uniformly distributed in the TiO<sub>2</sub> lattice [14]. Photocatalytic activity appeared under both UV and visible-light irradiation, and the activity depended on the concentration of iron dopant [15].

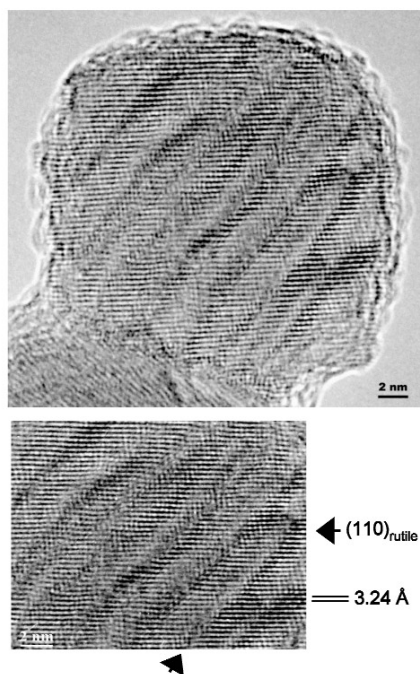


**Fig. 5** HRTEM image of a highly iron-doped nanocrystallite with  $R_{\text{Fe/Ti}} = 0.2$ .

The limit on the amount of Eu<sup>3+</sup> that can be doped into the TiO<sub>2</sub> lattice was 0.5 at %. Above that, Eu<sub>2</sub>Ti<sub>2</sub>O<sub>7</sub> pyrochlore was formed. Such a phenomenon is reasonable considering the very large size discrepancy between Ti<sup>4+</sup> (0.0605 nm for 6-fold coordination) and Eu<sup>3+</sup> (0.0947 nm for 6-fold coordination) ions. Figure 6 shows typical emission spectra of the TiO<sub>2</sub>: Eu<sup>3+</sup> nanoparticles as well as those of pure Eu<sub>2</sub>O<sub>3</sub> and Eu<sub>2</sub>Ti<sub>2</sub>O<sub>7</sub> under 325-nm He–Cd laser excitation [16]. It is the <sup>5</sup>D<sub>0</sub> → <sup>7</sup>F<sub>2</sub> transition that gives the sharp red color. The Eu<sup>3+</sup>-doped samples exhibited emissions clearly different from those of Eu<sub>2</sub>O<sub>3</sub> and Eu<sub>2</sub>Ti<sub>2</sub>O<sub>7</sub>, in terms of peak positions and peak shapes, implying different local environments. Efficient nonradiative energy transfer from the TiO<sub>2</sub> host to Eu<sup>3+</sup> ions, which has seldom been reported in nanoparticles or thin films of the same system obtained by wet-chemical methods, was confirmed through combined studies of excitation, UV–vis absorption, and photoluminescence spectroscopy.

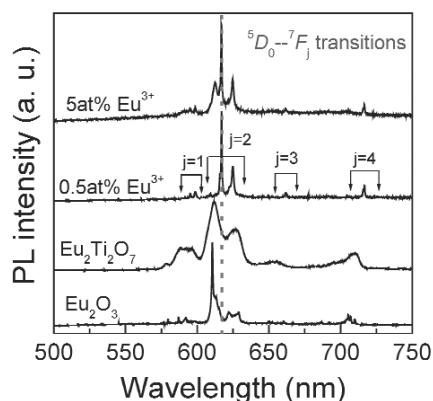


**Fig. 6** Emission spectra of  $\text{Eu}^{3+}$ -doped  $\text{TiO}_2$  nanopowders compared with those of  $\text{Eu}_2\text{O}_3$  and  $\text{Eu}_2\text{Ti}_2\text{O}_7$ .

## CONCLUSION—NANOPARTICLE APPLICATIONS

Applications of highly functional nanoparticles are thought to require nanoparticles structured in the forms of (1) dispersoids, (2) fillers, or (3) patterns (Fig. 7). For example, the red, green, and blue fluorescent particles used in plasma displays are currently fluorescent particles several micrometers in diameter produced by the solid-phase method by comminution. However, if we use even smaller fluorescent nanoparticles with sizes of a few tens of nanometers with excellent dispersion, the resolution dramatically improves and light scattering decreases. This should lead to high energy efficiency. Similarly, the absorption properties of electromagnetic wave absorbers in the gigahertz range and lower frequency ranges used in mobile devices dramatically improved with the use of magnetic nanoparticles thoroughly dispersed in plastic matrices.

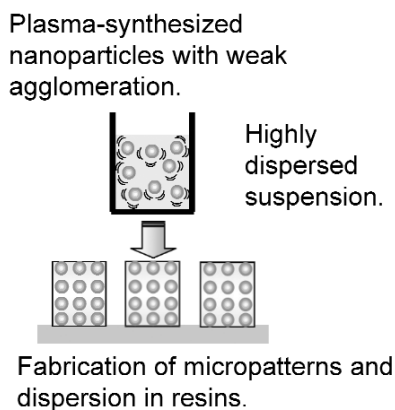


**Fig. 7** Controlled dispersion for creating functional nanostructures.

Consequently, whether using the liquid phase or vapor method for synthesis, the most important tasks at present are to achieve good crystallinity of the nanoparticles, provide additional functions through composition control, prevent aggregation by controlling surface properties, and prepare completely dispersed dispersoids. In situ dispersion is expected to become a key word, regardless of the synthesis method used.



In thermal plasma processing, nanoparticles are formed through coagulation from the vapor phase. The thermal plasma method, though similar to the spray pyrolysis method and the flame spray method, can produce highly crystalline nanoparticles with little surface residue because the synthesis temperature is far higher. As high crystallinity is related to functionalization and surface control for dispersion, thermal plasma processing is expected to make a significant contribution to nanoparticle applications. Furthermore, the SEM photos in Fig. 3 show that the plasma-synthesized nanoparticles are spherical and hardly agglomerated. We are now investigating ways of fabricating functional structures composed of well-dispersed nanoparticles.

## REFERENCES

1. R. Ye, T. Ishigaki, J. Jurewicz, P. Proulx, M. I. Boulos. *Plasma Chem. Plasma Process.* **24**, 555 (2004).
2. Y.-L. Li, T. Ishigaki. *J. Am. Ceram. Soc.* **84**, 1929 (2001).
3. M. I. Boulos. *J. Therm. Spray Technol.* **1**, 33 (1992).
4. Y.-L. Li, T. Ishigaki. *Chem. Mater.* **13**, 1577 (2001).
5. Y.-L. Li, T. Ishigaki. *Chem. Phys. Lett.* **367**, 561 (2003).
6. T. Ishigaki, Y.-L. Li, E. Kataoka. *J. Am. Ceram. Soc.* **86**, 1456 (2003).
7. T. Ishigaki, S.-M. Oh, J.-G. Li, D.-W. Park. *Sci. Technol. Adv. Mater.* **6**, 111 (2005).
8. J.-G. Li, H. Kamiyama, X. H. Wang, Y. Moriyoshi, T. Ishigaki. *J. Eur. Ceram. Soc.* **26**, 423 (2006).
9. J.-G. Li, T. Ishigaki, M. Ikeda, R. Ye, Y. Moriyoshi. *J. Phys. D: Appl. Phys.* **40**, 2348 (2007).
10. Y.-L. Li, T. Ishigaki. *J. Phys. Chem. B* **108**, 15536 (2004).
11. S.-M. Oh, J.-G. Li, T. Ishigaki. *J. Mater. Res.* **20**, 529 (2005).
12. Y.-L. Li, T. Ishigaki. *J. Cryst. Growth* **242**, 511 (2002).
13. X. H. Wang, J.-G. Li, H. Kamiyama, M. Katada, N. Ohashi, Y. Moriyoshi, T. Ishigaki. *J. Am. Chem. Soc.* **127**, 10982 (2005).
13. K. Yamaura, X. H. Wang, J.-G. Li, T. Ishigaki, E. Takayama-Muromachi. *Mater. Res. Bull.* **41**, 2080 (2006).
14. X. H. Wang, J.-G. Li, H. Kamiyama, Y. Moriyoshi, T. Ishigaki. *J. Phys. Chem. B* **110**, 6804 (2006).
15. J.-G. Li, X. H. Wang, K. Watanabe, T. Ishigaki. *J. Phys. Chem. B* **110**, 1121 (2006).